CONF-800744--1

OPTICAL IMAGE STORAGE IN ION IMPLANTED PLZT CERAMICS*

P. S. Peercy and C. E. Land
Sandia National Laboratories†
Albuquerque, New Mexico 87185

MASTER

Abstract

We have demonstrated that optical images can be stored in transparent lead-lanthanum-zirconate-titanate (PLZT) ceramics by exposure to near-uv light with photon energies greater than the band gap energy of $\sim$ 3.35 eV. The image storage process relies on optically induced changes in the switching properties of ferroelectric domains (photoferroelectric effect). Stored images are nonvolatile but can be erased by uniform UV illumination and simultaneous application of an electric field. Although high quality images, with contrast variations of $\geq$ 100:1 and spatial resolution of $\sim$ 10 μm, can be stored using the photoferroelectric effect, relatively high exposure energies ($\sim$ 100 mJ/cm^2) are required to store these images. This large exposure energy severely limits the range of possible applications of nonvolatile image storage in PLZT ceramics.

We have recently found from studies of H, He, and Ar implanted PLZT that the photosensitivity can be significantly increased by ion implantation into the surface to be exposed. For example, the photosensitivity after implantation with 5×10^{14} 500 keV Ar/cm^2 is increased by about three orders of magnitude over that of unimplanted PLZT. The image storage process and the effect of ion implantation is presented along with a phenomenological model which describes the enhancement in photosensitivity obtained by ion implantation. This model takes into account both light- and ion implantation-induced changes in conductivity and gives quantitative agreement with the measured changes in the coercive voltage with light intensity for ion implanted PLZT.

*This article sponsored by the U. S. Department of Energy under Contract DE-AC04-76-DP00789 and the U. S. Army Research Office.

†A U. S. Department of Energy facility.

DISCLAIMER

I. INTRODUCTION

Image storage[1] using the intrinsic[2] photoferroelectric (PFE) effect in PLZT (lead-lanthanium-zirconate-titanate) ceramics was first reported in 1976. The PFE effect is characterized by photoinduced changes in the effective ferroelectric (FE) coercive field, and these changes are used to store a nonvolatile space charge field E_{sc} in FE phase PLZT by switching the remanent polarization P while simultaneously exposing one surface of the ceramic to near UV light containing band gap (3.35 eV) or higher-energy photons. The reduction in the electric field required to reorient the FE domains in the presence of UV excitation is designated as photoassisted domain switching (PDS).[3,4]

Using PDS, images are stored in thin plates of FE phase PLZT which have transparent electrodes deposited on the two major surfaces. Images are stored by exposing one surface of the sample with the desired image with near UV light while simultaneously switching the ceramic through a portion of the FE hysteresis loop using an externally applied voltage. The image formed by the near UV light produces a spatially modulated E_{sc} which, under the action of the applied voltage, results in spatial modulation of the FE domain orientations. The FE domains retain their orientations after the light and voltage have been removed to produce a nonvolatile image. Because localized variations in FE domain orientations produce associated variations in light scattering and surface deformation strains,[5] the stored images may be viewed either in transmission or reflection using visible light. Although the images are nonvolatile and can be retained permanently in the absence of an applied voltage, they can be erased by switching the

remanent polarization through the FE hysteresis loop while simultaneously exposing the sample to spatially uniform near-UV light.

Another attractive feature of PLZT as an image storage medium is that the images can be switched from a positive to a negative or vice versa by switching the polarization from one saturation remanence to the other.[4,6] Partial switching can be used to enhance contrast in regions of the ceramic with a given level of exposure by the technique of baseline subtraction.[4,6]

The possible applications of PDS image storage in unmodified PLZT were severely limited by the relatively large exposure energy density required to store high quality images. The exposure energy W_{ex} (product of the near-UV light intensity I and the exposure time t) threshold for unimplanted PLZT is $\sim$ 85 mJ/cm^2. We have recently demonstrated that W_{ex} can be markedly reduced by ion implantation.[7] The 85 mJ/cm^2 threshold energy for unimplanted PLZT has been reduced to $\sim$ 10 μJ/cm^2 by implantation with Ar + Ne. This paper will summarize the ion implantation studies and present a phenomenological model[9] developed to account for the ion implantation-induced photosensitivity enhancement.

II. EXPERIMENT ARRANGEMENT

The PFE image storage devices are extremely simple and easy to fabricate. The device consists merely of a thin plate of polished PLZT 7/65/35, which denotes a solid solution with the composition $Pb_{0.93}La_{0.07}(Zr_{0.65}Ti_{0.35})_{0.983}O_3$ with transparent indium-tin oxide (ITO) electrodes sputter-deposited on the two major faces. The ITO electrodes have a thickness of $\sim$ 0.12 μm and a resistivity of $\sim$ 10 $\Omega/\square$.

Ion implantation was performed using a 300 keV Accelerators Inc. positive ion accelerator, and ion energies greater than 250 keV were achieved by

implantation of doubly charged ions. For most of the data presented in the present paper the ions were implanted before the ITO electrodes were deposited; however, we have recently found that more uniform implants, and therefore more uniform domain switching, can be obtained if a thin ($\sim$ 100 Å) ITO layer is deposited prior to implantation to prevent charge buildup. In this latter case, additional ITO is deposited after implantation to yield a total electrode thickness of 0.12 μm. A schematic illustration of the ion-implanted device is shown in Fig. 1. Typical device dimensions are 25 x 25 x 0.25 mm^3, although devices with much larger areas can be readily fabricated. Typical implant and absorption depths are $x_3 \lesssim 1$ μm and $x_2 \sim 10$ μm, respectively, and the remaining thickness $x_1 \sim 240$ μm is uneffected by either the implantation or illumination.

III. EXPERIMENTAL RESULTS

Nonvolatile images with gray scale ranges extending from an optical density of 0.15 to > 2.0 and with resolution as high as 40 line pairs per millimeter are routinely stored in PLZT using the intrinsic PFE effect. A photograph of an image stored in unimplanted PLZT is shown in Fig. 2. An example of the resolution achievable is given by the image of a resolution chart stored in Fig. 3. The photographs in this figure further illustrate the capability for altering images in PLZT after they are stored by the application of an external voltage. The photograph on the left is the image as stored whereas the photograph on the right shows the negative obtained by switching the remanent polarization after the image was stored. This switching is accomplished by the application of an appropriate voltage in the absence of UV illumination.

With the appropriate choice of the applied voltage, the contrast in regions of the image exposed at any given level can be enhanced as illustrated

by the photographs in Fig. 4. Figure 4A is a photograph of the step density transparency used to store the image of Fig. 4B. The calibrated density variation is 0.5 optical density per step. The average remanent polarization P_r of the ceramic of Fig. 4B was arbitrarily set at zero for reference purposes. When P_r was switched to -6.53 $\mu C/cm^2$, the maximum density step moved from position 1 in Fig. 4B to position 2 in Fig. 4C. As P_r was switched to increasingly negative values as shown in Figs. 4D, 4E, and 4F, the maximum density step moved from position 2 to positions 3, 4, and 5, respectively. This technique of baseline subtraction in the stored image may be used to modify and enhance the contrast of images stored in a PFE device.

While the use of PLZT for either temporary or long term image storage has many attractive features including manipulation of the stored image for contrast enhancement, the relatively large W_{ex} of 100 to 300 mJ/cm^2 required to store high quality images severely limits the applications of PLZT. We have found that W_{ex} can be reduced significantly when the electrical and dielectric properties of the near-surface region are altered by ion implantation as will be discussed below. The atomic depth distribution and the depth distribution of energy deposited into electronic and atomic processes are shown in Fig. 5 for 200 keV H implanted into PLZT. The curves in Fig. 5 were calculated using Brice's codes[8] which yield a projected range of 1.03 μm for 200 keV H and the maximum in the energy deposited into atomic process occurs at 0.9 μm.

The dramatic increase in photosensitivity afforded by ion implantation is illustrated by the photograph shown in Fig. 6. The lower half of the ceramic was implanted with 2×10^{16} 200 keV H/cm^2 and the upper half was not implanted. Both the upper unimplanted and lower implanted regions of the surface were exposed identically (20 mJ/cm^2) during image storage. As can

be seen from the photograph, a high quality image is stored in the implanted region at exposure levels insufficient to store a detectable image in unimplanted PLZT. It should also be noted that no degradation in the image quality is observed in the implanted material; in fact, for uniform implants, the image quality is generally higher than that for unimplanted PLZT.

We have found that the ion implantation-induced photosensitivity enhancement results from the disorder produced by energy the implanted ions deposit into atomic processes. The primary effect of the disorder is to decrease the dark conductivity of the implanted region relative to the unimplanted conductivity and to alter the photoconductivity. The 200 keV H implants deposit $\lesssim$ 0.5% of the ion energy into atomic processes. A much higher fraction of the ion energy is deposited into atomic processes with heavy ions than with H although the range of heavy ions decreases with increasing mass for the same energy. Since the ion implantation-produced enhancement also depends on the thickness of the implanted layer, as will be discussed below, we have used co-implants of Ar and Ne to extend the disordered region to $\sim$ 0.5 μm. The effect of these Ar + Ne co-implants are illustrated by the hysteresis loops shown in Figs. 7 and 8.

A hysteresis loop for an unimplanted, unilluminated PLZT sample 0.25 μm thick is shown in Fig. 7. For this thickness, the threshold field for domain switching, $E_{th} \sim 3.5 \times 10^5$ V/m occurs at an applied threshold voltage V_{th} of $\sim$ 100 V. The coercive field $E_c = 4.1 \times 10^5$ V/m, where the polarization is zero, occurs at a coercive voltage $V_{c,u} \tilde{=} 120$ V. For the Ar + Ne co-implanted sample (Fig. 8), the dark coercive voltage (curve 0) has been increased to $V_{c,i}(0) \tilde{=} 275$ V. At this applied voltage, the electric field in the underlying unimplanted region of the sample is equal to E_c of unimplanted PLZT. The curves numbered 1 through 15 were taken with increasing intensity I of

near-UV illumination ranging from 1 $\mu W/cm^2$ (curve 1) to 98 mW/cm^2 (curve 15). The decrease in V_c with I is used for quantitative measurement of the photosensitivity as discussed below.

To store an image in the sample of Fig. 8, a switching voltage of, e.g., 150 V would be applied to the ceramic without illumination. Since this voltage is less than the threshold voltage for domain switching, no FE domains would be reoriented. The image to be stored would then be exposed on the implanted surface using near-UV light. As can be seen from the data in Fig. 8, the simultaneous application of UV light and the switching voltage will reorient domains under the exposed regions of the ceramic. Since the domain switching is proportional to I, an image which faithfully reproduces the gray scale will be stored in the ceramic plate.

IV. MODEL CALCULATIONS

In this section we present a simple phenomenological model[9] to describe both the photoinduced reduction of V_c which governs the storage process and the ion-implantation enhancement of the photosensitivity. Since the photon energy is greater than the bandgap energy, the light will generate charge carriers and increase the conductivities in regions (2) and (3) of Fig. 1. To simplify the analysis, we first consider the case for unimplanted PLZT for which $x_3 = 0$ and $d = x_1 + x_2$. At the instant the voltage V is applied ($t = 0$), the electric fields in regions (1) and (2) are governed by

$$D_1 = D_2, \text{ or } \varepsilon_1 E_1 = \varepsilon_2 E_2 \quad , \tag{1}$$

where D_1, D_2 are electric displacements and ε_1, ε_2 are relative dielectric permittivities. For $t \to \infty$, the continuity equation reduces to

$$j_1 = j_2, \text{ or } \sigma_1 E_1 = \sigma_2 E_2 \quad , \tag{2}$$

where j_1, j_2 are current densities, and σ_1, σ_2 are conductivities. For the experiments under consideration we are interested in the long time (essentially dc) behavior governed by Eq. (2).

To estimate the effect of illumination on the conductivity σ_2, we assume that the photoexcited carrier concentration is dominated by intrinsic photoconductivity. Under this assumption the light-induced electron concentration N will obey

$$dN/dt = aI - bN^2 \tag{3}$$

where aI and bN^2 govern carrier excitation and recombination, respectively. For constant I, dN/dt = 0, so that N, and the attendant changes in σ, are proportional to $I^{\frac{1}{2}}$. For intrinsic photoconductivity we thus write for region (2)

$$\sigma_2(I) = \sigma_1 + A\sqrt{I(x)} \ . \tag{4}$$

If the conductivity is dominated by one type of carrier, A is given by $A = (a/b)\, e \cdot \mu$ where e and μ are the electronic charge and carrier mobility, respectively. It should be noted that $\sigma_2(I)$ is an exponentially decreasing function of depth x from the surface with a fall-off governed by the absorption length α^{-1} of $\sim$ 10 μm for λ = 365 nm.[9]

The applied voltage V is dropped across the sample according to

$$V = \int_o^{x_2} E_2(x)\,dx + \int_{x_2}^{d} E_1\,dx \tag{5}$$

which, under the above assumptions, can be solved to yield E(x) throughout the sample, as

$$V(I) = E_1 d \left\{ 1 + \frac{2}{\alpha d} \ln \left[\frac{\sigma_1 + A\sqrt{I_o} \exp(-\alpha x_2/2)}{\sigma_1 + A\sqrt{I_o}} \right] \right\} \qquad (6)$$

when the field E_1 is taken to be constant throughout region (1). We could have written a general expression for E(x) throughout depth d and solved Eq. (5) to yield an equation identical to Eq. (6) with x_2 replaced by d. However, the purpose of dividing d into the regions x_1 and x_2 was to permit the solution to be expanded for small x_2, where x_2 is the depth for which $\sigma_2 >> \sigma_1$. Although this expansion requires an additional fitting parameter, the resulting equations are valuable for optimizing the device performance. We thus expand Eq. (6) for small x_2 to yield

$$V_u(I) \cong \left[1 + \left(\frac{\sigma_1}{\sigma_1 + A\sqrt{I_o}} \right) \frac{x_2}{x_1} \right] E_1 x_1 \quad . \qquad (7)$$

Two interesting features are evident from Eq. (7). Since I decreases rapidly with x, the depth x_2 over which there is an appreciable change in σ changes with I. Secondly, in the above approximation, light-induced changes in the conductivity in region (2) have a second-order effect on the voltage required to attain a given field in the dark region (1). Physically this dependence reflects the fact that the low-conductivity bulk region governs the current through the sample. Once the conductivity of region (2) appreciably exceeds that of region (1), further increases in the conductivity of region (2) have only a small effect on the total current. Assuming that Eq. (7) holds at the coercive field for the present experimental conditions and postulating that the depth x_2 is governed by Eq. (4), within the framework of the above approximations Eq. (7) becomes

$$V_{c,u}(I) = E_{c,u}(0)d\left(1 - \frac{x_2}{d}\right)\left[1 + \left(\frac{x_2}{d-x_2}\right)\left(\frac{\sigma_1}{\sigma_1+A\sqrt{I_o}}\right)\right]$$

$$\tilde{=} V_{c,u}(0)\ (1 - B\sqrt{I})\left[1 + \frac{B\sqrt{I}}{1+A\sqrt{I}/\sigma_1(0)}\right] \quad , \tag{8}$$

where the approximate form of Eq. (8) derives from setting $x_2/(d-x_2) = x_2/d \equiv B\sqrt{I}$ in the second-order term. The subscript c denotes that $V_u(I)$ is evaluated at the coercive field $E_{c,u}$, and $E_{c,u}(0)$ is taken to be a constant parameter of the material, i.e., we assume a critical field is required to switch the unilluminated ceramic. B is defined by B = 1/d times a parameter analogous to A in Eq. (4). The physical significance of B is that $B\sqrt{I}$ is the value of x_2 for which $E_2 << E_1$.

We next consider the effect of ion implantation. Ion implantation changes ϵ and σ in a well-defined near-surface ($\lesssim$ 1 μm) region denoted as (3) in Fig. 1 and can have marked effects on V_c for both the illuminated and the unilluminated conditions. Straightforward solution of equations analogous to Eqs. (2) and (5) for I = 0 yields

$$V_i(0) = \left(1 + \frac{\sigma_1}{\sigma_3(0)}\frac{x_3}{x_1}\right)E_1x_1 \quad , \tag{9}$$

where the subscript i denotes implanted PLZT and σ_3 is taken to be uniform over the depth x_3. From Eq. (9) it is apparent that the increase in the coercive voltage $V_{c,i}$ at I = 0 produced by ion implantation results from a decrease in the dark conductivity $\sigma_3(0)$ of region (3). For example, for 5×10^{14} 400 keV Ar/cm^2, which has $x_3 \cong 0.5$ μm, we find that $\sigma_1/\sigma_3(0) \cong 340$.

For I ≠ 0, if we approximate the sample by three regions, analogous to a two-region approximation for unimplanted PLZT, Eqs. (2), (4), and (5)

can be extended and solved to yield $V_{c,i}(I)$ in terms of the dark coercive field of region (1), $E_{c,u}(0)$. Assuming that the photoconductivity is intrinsic in the implanted region also, one finds

$$V_{c,i}(I) = V_{c,u}(I) + V_{c,u}(0)\ (1-B\sqrt{I_o})\left(\frac{1}{1+C\sqrt{I_o}/\sigma_3}\right)\frac{\sigma_1 x_3}{\sigma_3 x_1} \quad , \qquad (10)$$

where $V_{c,u}(I)$ is given by Eq. (8) and C is analogous to A in Eq. (4) but refers to implanted material.

V. DISCUSSION

If the microscopic parameters such as a, b, μ, etc., were known for PLZT, the parameters introduced in Section IV could be evaluated to calculate $V_c(I)$ from first principles. Unfortunately, these parameters are not known, so we treat the parameters A, B and C in Eqs. 8 and 10 as adjustable parameters to determine if the intensity dependence of V_c is adequately described by the model. $V_c(0)$ is directly measured at I = 0 and the parameters A and B in Eq. (8) can be readily evaluated from the data. The solid curve for the unimplanted sample in Fig. 9 was calculated for: $A/\sigma_1(0) = 2.0\ (mW/cm^2)^{-\frac{1}{2}}$ and $B = 0.022\ (mW/cm^2)^{-\frac{1}{2}}$. As can be seen for Fig. 9, Eq. (8) gives a good fit to the measured $V_{c,u}(I)$ for unimplanted PLZT throughout the intensity region 1 $\mu W/cm^2 \leq I \leq 100\ mW/cm^2$ investigated.

Two variables of Eq. (10) which depend directly on the conditions of ion implantation are x_3 and σ_3. To maximize photosensitivity, Eq. (10) indicates that the ion damage depth x_3 should be increased and that the dark conductivity $\sigma_3(0)$ in the implantation region should be minimized. The damage depth x_3 is increased either by implanting ions with lower mass or by implantation at higher energies; $\sigma_3(0)$ is reduced by maximizing implantation damage with more massive ions. Both of these dependences have been verified experimentally.

The photosensitivity increase obtained with 500 keV Ar compared to 400 keV Ar (Fig. 9) illustrates the x_3 dependence. The lower photosensitivity for 200 keV He,[7] which has greater x_3 than does 500 keV Ar, reflects the damage dependence.

To describe the dependence of the coercive voltage on I for ion-implanted PLZT, we use the parameters obtained for unimplanted PLZT together with $\sigma_1 x_3/\sigma_3 x_1$ evaluated from Eq. (9) at I = 0 and C of Eq. (10) evaluated at some point on the $V_{c,i}(I)$ curve. Calculated $V_c(I)$ dependences for H, Ar, and Ar + Ne implants are compared with the measured dependences in Fig. 9. It is apparent from the curves in Fig. 9 for ion-implanted PLZT that Eq. (10) gives a reasonable description throughout the five decades in I which were measured. The curves for the Ar implants were calculated using the above parameters and $C/\sigma_3(0) = 0.80\ (mW/cm^2)^{-\frac{1}{2}}$. Identical parameters were used for the 400 and 500 keV Ar implants, with the exception of x_3 which was adjusted to account for the differences in range. The fact that both curves give accurate fits to the data lends further support for this model.

The ion-implantation induced enhancement in photosensitivity is summarized in Fig. 10 where the change in coercive voltage ΔV_c is plotted as a function of I for different implanted ions. Empirically we find that the image storage threshold for a one second exposure occurs at $\Delta V_c \sim -25V$, independent of the implanted species. The image storage threshold may thus be read directly from the curves in Fig. 10, and has been decreased from 85 mJ/cm^2 in unimplanted PLZT to $\sim$ 45 $\mu J/cm^2$ for co-implants of 5×10^{14} 500 keV Ar + 1.5×10^{15} 400 keV Ne. Very recently, we have further reduced[10] the threshold energy to $\sim$ 10 $\mu J/cm^2$ with co-implants of 500 keV Ne and 350 keV Ar which yields a more uniform damage distribution than the co-implants reported in Fig. 10. We should also note that implantation with chemically active ions can be used to shift the absorption spectrum so that visible

light can be used for image storage. For example, preliminary measurements demonstrate that light from an incandescent bulb can be used to store high-quality images in Al-implanted PLZT.

Acknowledgements:

The authors wish to thank I. D. McKinney for fabrication of the image storage devices and M. E. Wilkins for assistance with the ion implantations.

REFERENCES

1. C. E. Land and P. S. Peercy, 1976 IEEE-SID Biennial Display Conf. Proc., 71 (1976).

2. F. Micheron, Ferroelectrics 12, 41 (1976).

3. C. E. Land and P. S. Peercy, Ferroelectrics 22, 677 (1978).

4. C. E. Land, Optical Engrg. 17, 317 (1978).

5. C. E. Land, Ferroelectrics 7, 45 (1974).

6. C. E. Land and P. S. Peercy, 1978 SID Intl. Symp. Dig. of Tech. Papers, 9, 14 (April 1978).

7. C. E. Land and P. S. Peercy, Appl. Phys. Lett. 37, 39 (1980).

8. D. K. Brice, Rad. Eff. 6, 77 (1970); J. Appl. Phys. 46, 3385 (1975).

9. P. S. Peercy and C. E. Land, Appl. Phys. Lett. (To be published).

10. C. E. Land and P. S. Peercy (unpublished).

FIGURE CAPTIONS

Fig. 1. Schematic illustration of a PLZT optical image storage device showing the implanted depth x_3 and the illuminated depth x_2.

Fig. 2. Examples of photographs stored in unimplanted, 5 μm grain size PLZT 7/65/35. (A) illustrates storage of an image with variable gray scale, and (B) is a resolution chart with approximately 50% modulation at 20 lines/mm.

Fig. 3. Illustration of the ability to electrically switch a stored image from a positive to a negative. The photograph on the left is the image as s red whereas the photograph on the right shows the negative obtained by switching the remanent polarization to the opposite polarity.

Fig. 4. Illustration of the contrast enhancement which results from partial switching of the remanent polarization.

Fig. 5. Calculated energy (eV/Å) deposition and hydrogen distribution for 200 keV protons in PLZT 7/65/35.

Fig. 6. Photographs of resolution charts stored in PLZT 7/65/35 plates. The lower half of plate (A) was implanted with 4×10^{16} 200 keV H/cm^2; the lower half of (B) was implanted with 2×10^{16} 200 keV H/cm^2. The upper half of each plate was unimplanted. The images were exposed uniformly on both the upper and lower halves of each plate at $W_{ex} \sim 20$ mJ/cm^2.

Fig. 7. Hysteresis loop for unimplanted, unilluminated PLZT 7/65/35.

Fig. 8. Hysteresis loops for Ar + Ne co-implanted PLZT at various uniform light intensities ranging from 1 $\mu W/cm^2$ (curve 1) to $\sim$ 100 mW/cm^2 (curve 15). Curve 0 is for I = 0.

Fig. 9. Comparison between the model calculations and measurements of $V_c(I)$ for unimplanted and H-, Ar-, and Ar + Ne co-implanted PLZT 7/65/35.

Fig. 10. Plots of the light induced change in coercive voltage, ΔV_c, versus light intensity for 1 $\mu J/cm^2 \leq I \leq 100$ mW/cm^2. The image storage threshold occurs for $V_c \tilde{=} -25V$ and the threshold exposure energies for the different implants are noted on the graph.

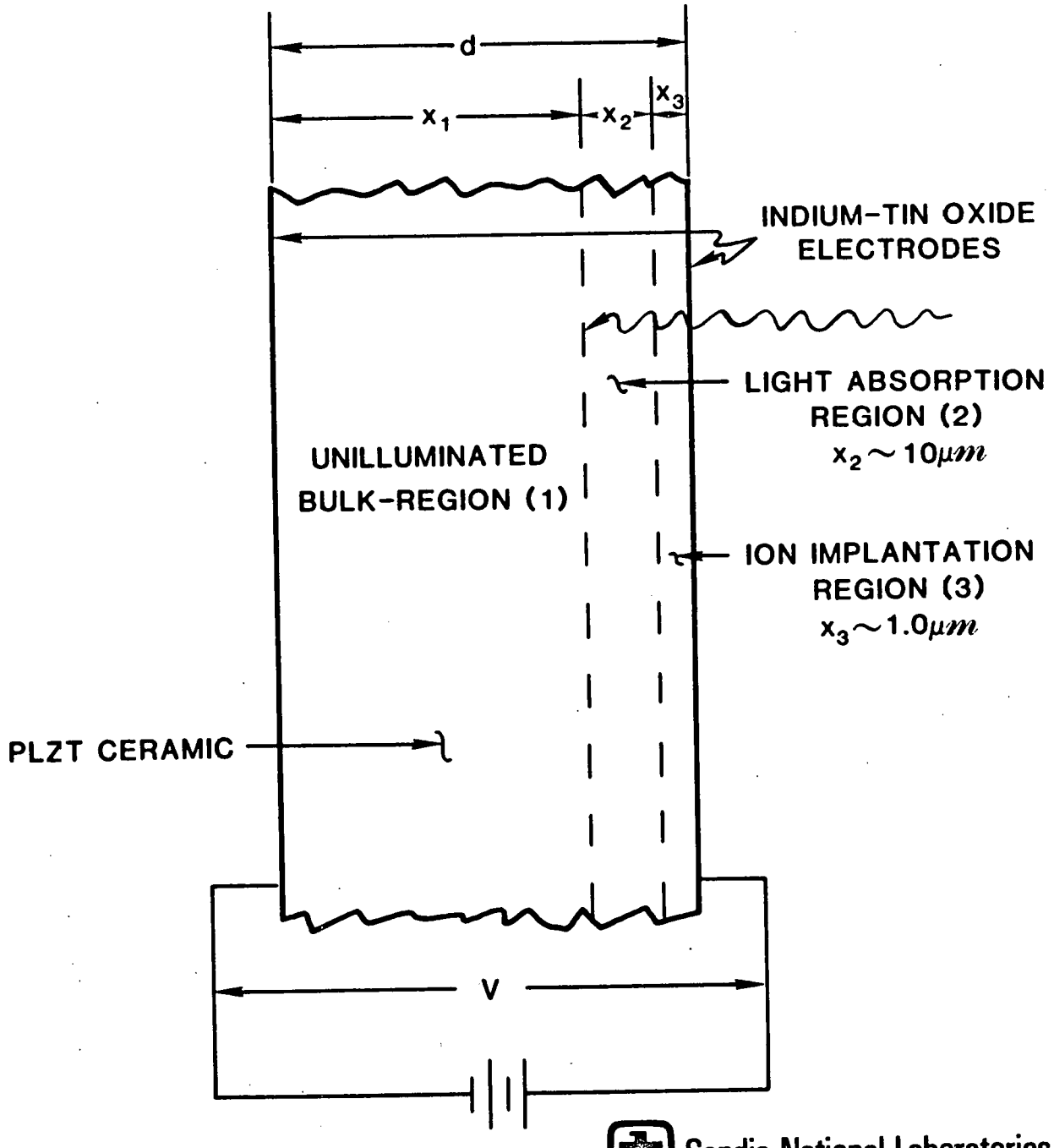

Sandia National Laboratories

A

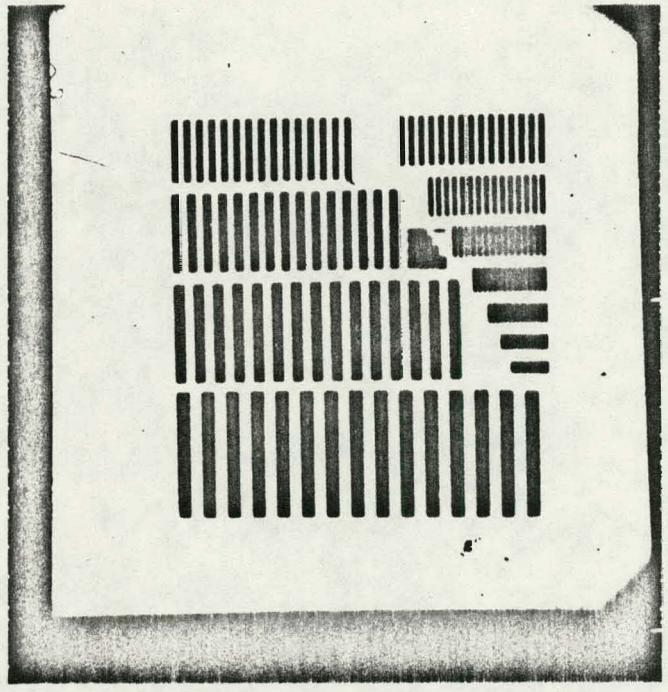

B

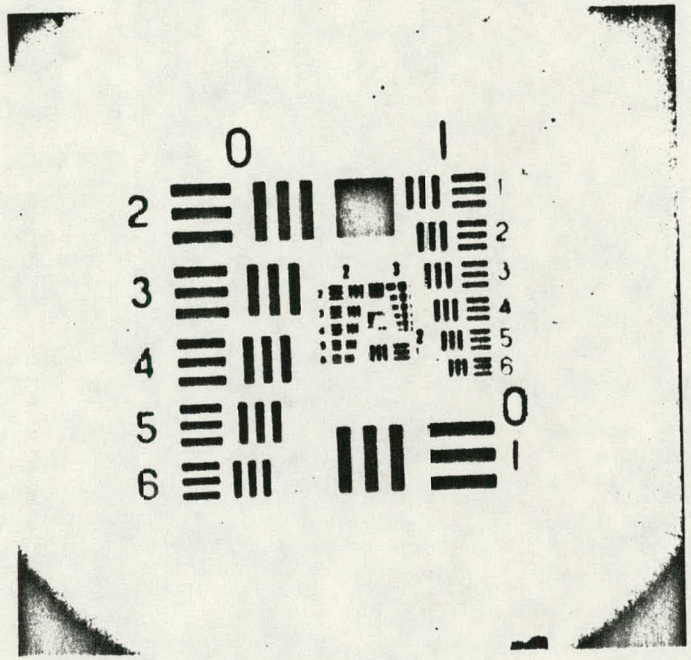

A

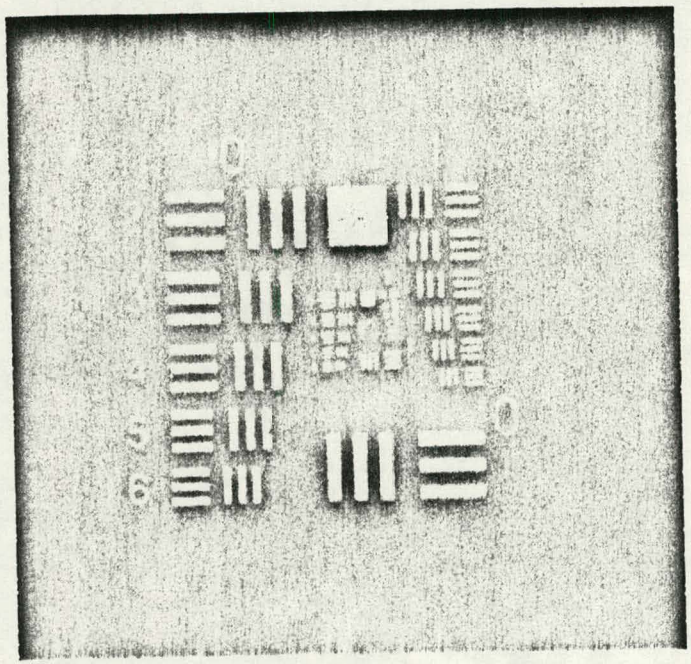

B

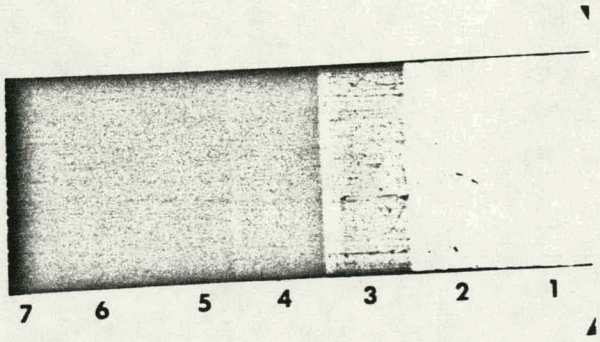

(A) Input Step Density Scale

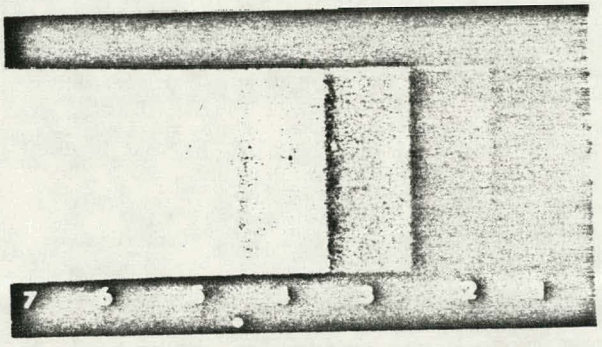

(B) Stored Negative of (A)
$P_R(AV) = 0$

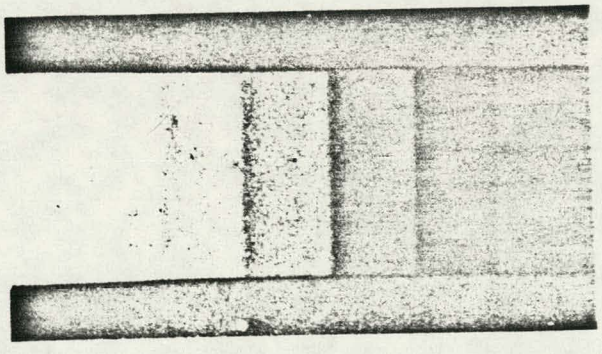

(C) Image in (B) After Switching to $P_R(AV) = -6.53\ \mu C/cm^2$

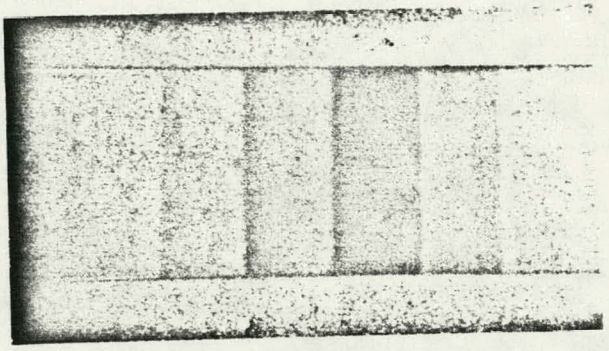

(D) Image in (B) After Switching to $P_R(AV) = -12.30\ \mu C/cm^2$

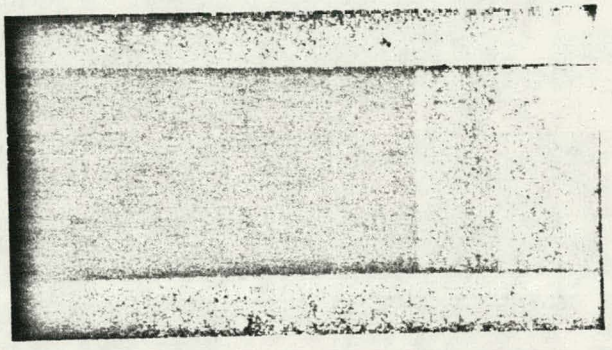

(E) Image in (B) After Switching to $P_R(AV) = -17.35\ \mu C/cm^2$

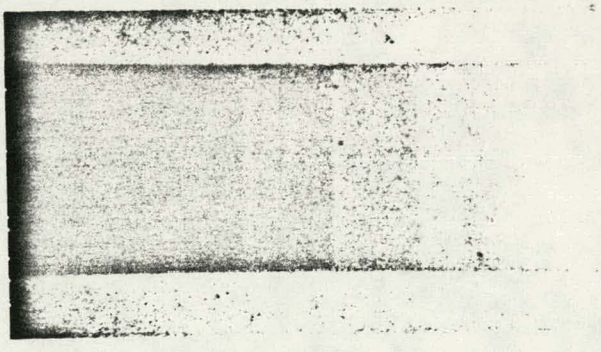

(F) Image in (B) After Switching to $P_R(AV) = -21.5[illegible]\ \mu C/cm^2$

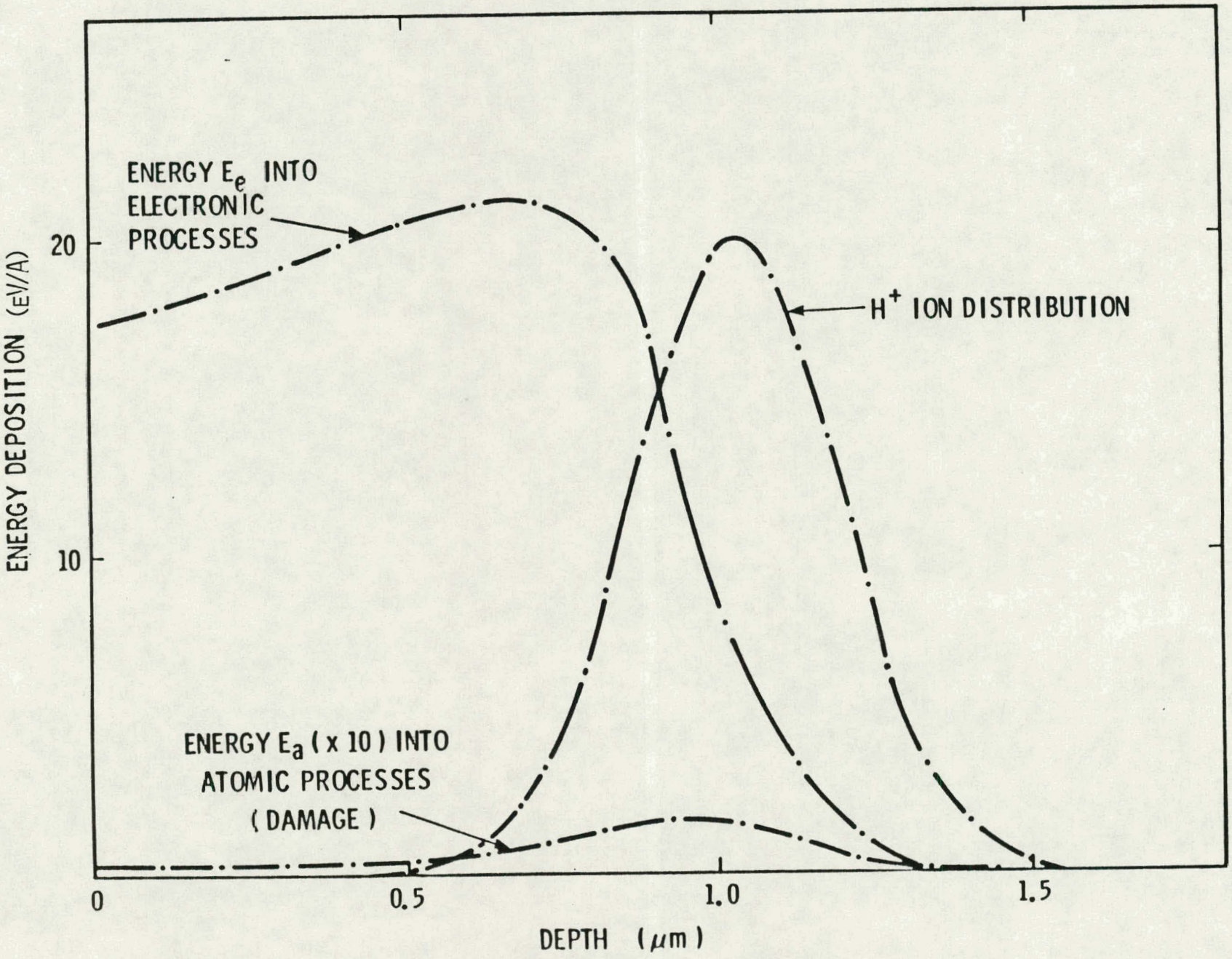
ENERGY E_e INTO
ELECTRONIC
PROCESSES
H^+ ION DISTRIBUTION
ENERGY E_a (x 10) INTO
ATOMIC PROCESSES
(DAMAGE)
ENERGY DEPOSITION (eV/A)
20
10
0
0.5
1.0
1.5
DEPTH (μm)

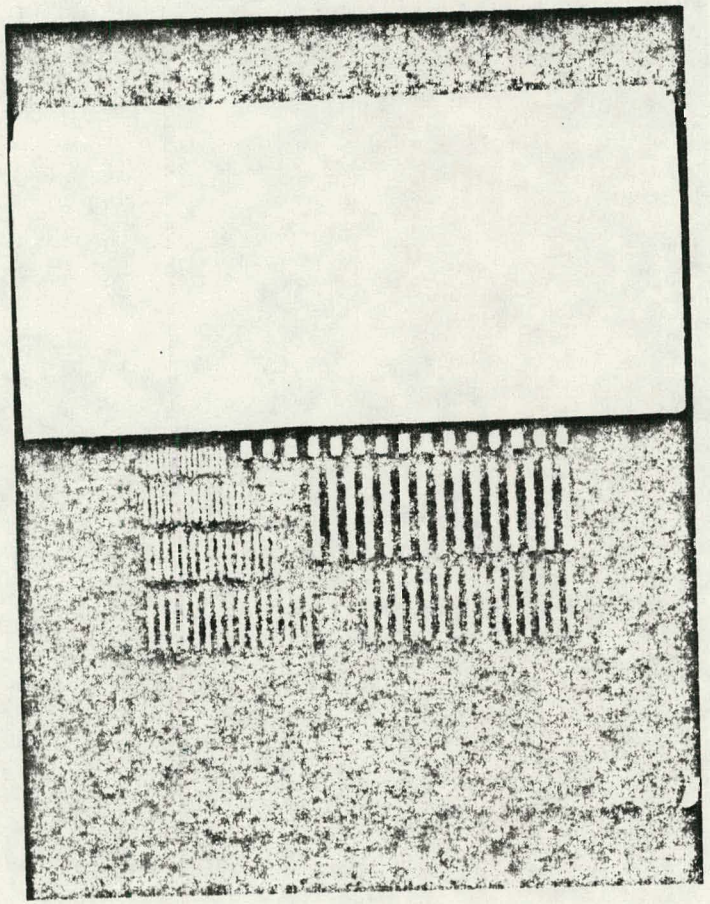

(A)

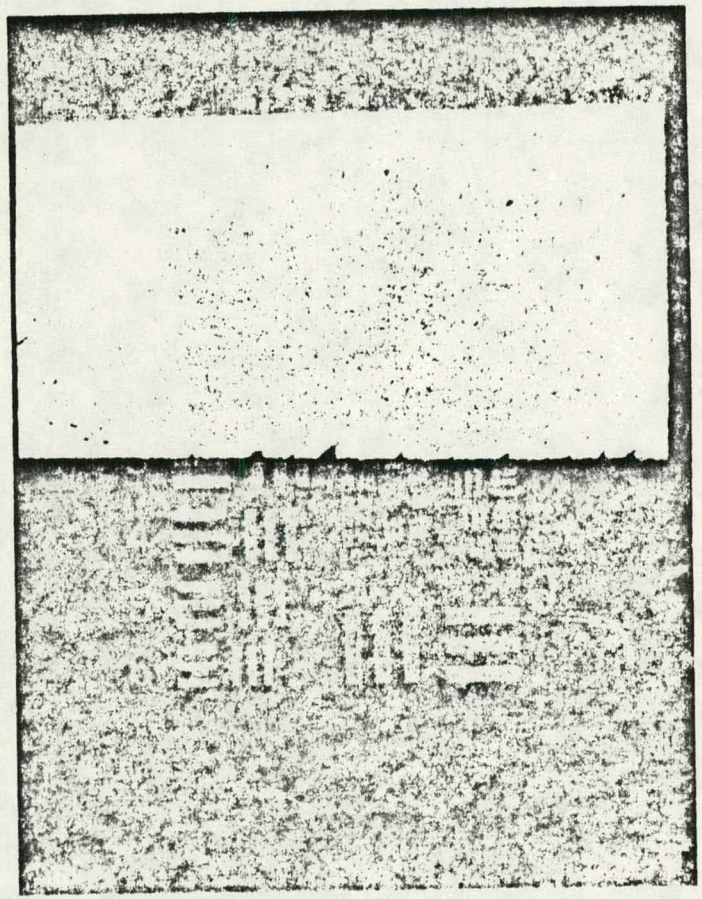

(B)

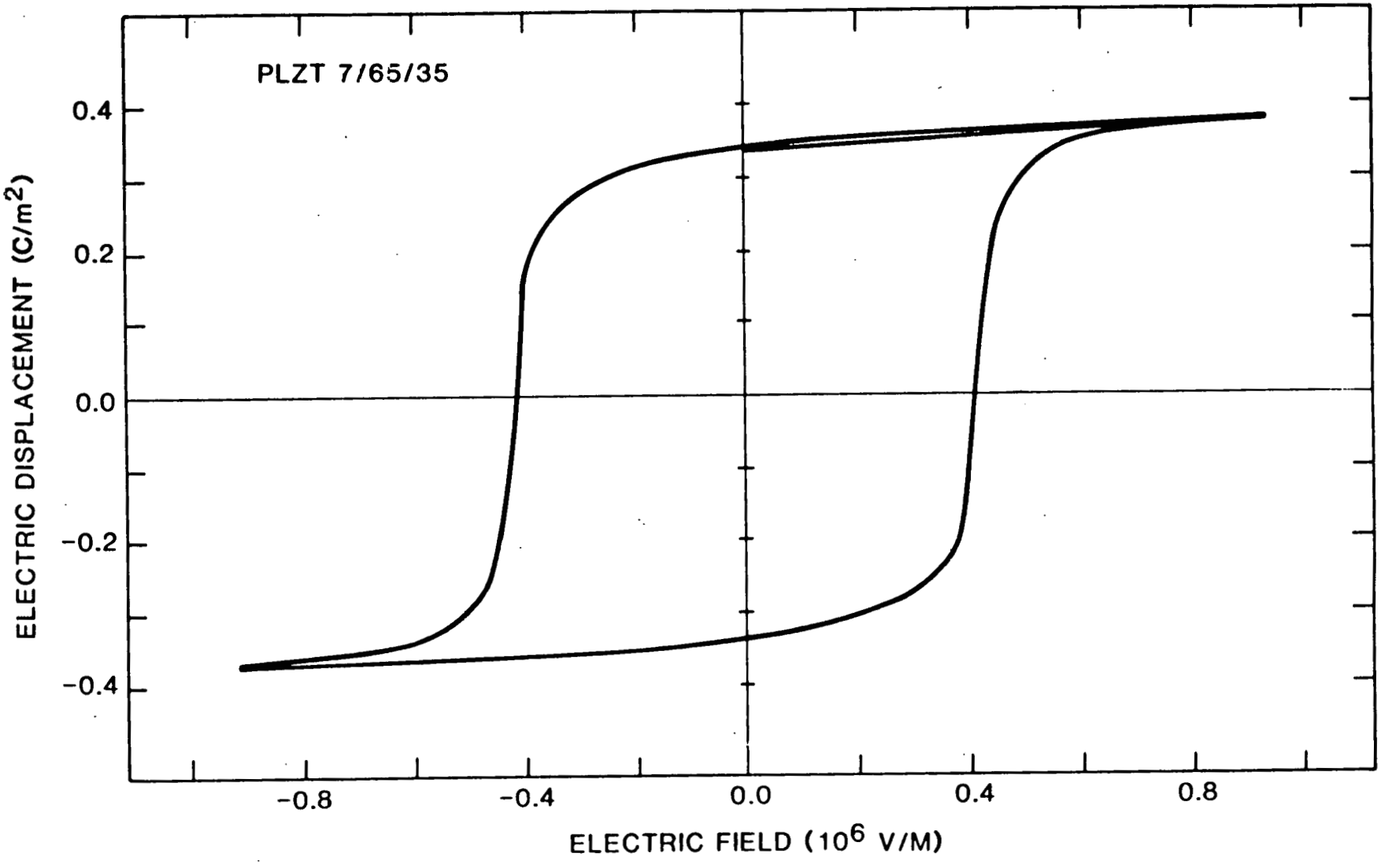

Sandia National Laboratories